AGU PUBLICATIONS

JGR

Journal of Geophysical Research: Atmospheres

RESEARCH ARTICLE
10.1002/2016JD026242

Key Points:
- Current precipitation extremes were determined in the dry and wet regions of China using observations, CMIP5s, and RCMs
- Precipitation extremes over the dry regions of China had positive regression coefficients versus the SST of the ETP

Supporting Information:
- Supporting Information S1

Correspondence to:
P. Qin,
qinpeihua@mail.iap.ac.cn

Citation:
Qin, P., and Z. Xie (2017), Precipitation extremes in the dry and wet regions of China and their connections with the sea surface temperature in the eastern tropical Pacific Ocean, *J. Geophys. Res. Atmos.*, *122*, 6273–6283, doi:10.1002/2016JD026242.

Received 18 NOV 2016
Accepted 8 JUN 2017
Accepted article online 11 JUN 2017
Published online 26 JUN 2017

Precipitation extremes in the dry and wet regions of China and their connections with the sea surface temperature in the eastern tropical Pacific Ocean

Peihua Qin[1] **and Zhenghui Xie**[1]

[1]State Key Laboratory of Numerical Modeling for Atmospheric Sciences and Geophysical Fluid Dynamics (LASG), Institute of Atmospheric Physics, Chinese Academy of Sciences, Beijing, China

Abstract We investigated the connections between the precipitation extremes during 1953–2002 in the dry and wet regions of China and the sea surface temperature (SST) in the eastern tropical Pacific Ocean (ETP; including El Niño–Southern Oscillation 1.2, 3, and 3.4 regions) based on two sets of observations, 17 Coupled Model Intercomparison Project Phase 5 (CMIP5) models, and nine regional climate model (RCM) results, which were downscaled using the RCM RegCM4. The grid cells with the lowest 30% nonmissing precipitation extremes were identified as the dry region, and those with the highest 30% comprised the wet region. Compared with observed extreme indices, the CMIP5 ensemble could simulate the temporal averages and spatial patterns of extreme indices in the dry and wet regions, where the temporal averages of the indices based on RCMs matched better with those of the observed indices. In the dry region of China, the extreme precipitation indices had positive regression coefficients versus the SST of the ETP for all data sets, but the linear relationships of the extreme indices with the SST were more complex in the wet region. Finally, we investigated the variations of the correlations of precipitation extremes with the SST of ETP in multiple RCM results and CMIP5 models, respectively.

1. Introduction

Precipitation extremes are of general interest due to their profound impacts on the economy, human safety, and the natural environment [*IPCC*, 2012]. Precipitation extremes exhibit high spatiotemporal variation in terms of both their frequency and intensity relative to the mean precipitation [*Donat et al*., 2013], so it is always difficult to detect extreme events and their underlying related mechanisms.

Numerous studies have focused on the detection and attribution of precipitation extremes [*Bellprat and Doblas-Reyes*, 2016]. The monitoring of precipitation extremes in the wet and dry regions of the world has increased [*Donat et al*., 2016], and precipitation extremes are known to be less sensitive to global warming over mountains relative to that over oceans and plains [*Shi and Durran*, 2016]. A physical analysis of the effects of key climatic factors (vertical velocity, saturation specific humidity, and surface temperature) on precipitation extremes was performed based on an extreme scaling formula that large upward vertical velocity and large derivative of the saturation specific humidity might cause strong intensity of precipitation extremes [*O'Gorman*, 2012; *O'Gorman and Schneider*, 2009]. In addition, heavy precipitation extremes exhibit increase during those periods with high temperature and decrease during cold periods [*Allan and Soden*, 2008; *Chan et al*., 2016] and the wet precipitation extremes are highly related to the mean precipitation, water vapor, and vertical wind [*Qin and Xie*, 2016].

Precipitation extremes are also affected profoundly by the sea surface temperature (SST) via changes in the atmospheric circulation, which is an important factor that affects water vapor and the wind, thereby leading to changes in precipitation [*Meehl et al*., 2007; *Sun et al*., 2015; *Ummenhofer et al*., 2015]. The SST has significant impacts on the mean climate [*Huang and Xie*, 2015; *Martin et al*., 2014; *Seager et al*., 2005; *Sun et al*., 2016], e.g., the global pattern of the impact of the El Niño–Southern Oscillation (ENSO) on precipitation [*Dai and Wigley*, 2000], precipitation anomalies in North America [*Castello and Shelton*, 2004] and South America [*Grimm*, 2011], the strong correlation between extreme precipitation in Europe and the Mediterranean SST [*Volosciuk et al*., 2016], and the relationships between changes in precipitation in China relative to the SST [*Tian et al*., 2016; *Zhang et al*., 2016]. Compared with temperature extremes, precipitation extremes are less spatially correlated with the global SST [*Alexander et al*., 2009]. *Donat et al*. [2014] found that precipitation extremes generally had stronger correlations with the North Atlantic Oscillation rather than with the ENSO

Table 1. Descriptions of the 17 CMIP5 Models Used in This Study

Model	Institution	Resolution (Longitude × Latitude ~ Level)
ACCESS1.0	Commonwealth Scientific and Industrial Research Organization and Bureau of Meteorology, Australia	192 × 145 L38
BCC-CSM1.1	Beijing Climate Center, China Meteorological Administration, China	128 × 64 L26(T42)
BNU-ESM	Beijing Normal University, China	128 × 64 L26(T42)
CanESM2	Canadian Centre for Climate Modelling and Analysis, Canada	128 × 64 L35(T63)
CCSM4	National Center for Atmospheric Research, USA	288 × 192 L26
CESM1-BGC	National Science Foundation (NSF), U.S. Department of Energy (DOE), and National Center for Atmospheric Research, USA	288 × 192
CNRM-CM5	Centre National de Recherches Meteorologiques, Meteo-France, France	256 × 128 L31(T127)
CSIRO-Mk3.6.0	Australian Commonwealth Scientific and Industrial Research Organization, Australia	192 × 96 L18(T63)
FGOALS-g2	LASG, Institute of Atmospheric Physics, Chinese Academy of Sciences, China	128× 60 L26
FGOALS-s2	LASG, Institute of Atmospheric Physics, Chinese Academy of Sciences, China	128 × 108 L26
GFDL-ESM2M	Geophysical Fluid Dynamics Laboratory, USA	144 × 90 L24
HadGEM2-ES	Met Office Hadley Centre, UK	192 × 145 L38
IPSL-CM5A-LR	L'Institut Pierre-Simon Laplace, France	96 × 96 L39
MIROC-ESM-CHEM	National Institute for Environmental Studies, The University of Tokyo, Japan	128 × 64 L80(T42)
MPI-ESM-LR	Max Planck Institute for Meteorology, Germany	192 × 96 L47(T63)
MRI-CGCM3	Meteorological Research Institute, Japan	320 × 160 L48(T159)
NorESM1-M	Norwegian Climate Centre, Norway	144 × 96 L26

in the Arab region. Both dry and wet events were predicted to increase moderately in California at the end of this century due to the enhanced relationship with the ENSO [*Yoon et al*., 2015]. However, the impact of the ENSO on extreme precipitation may differ among regions and it is asymmetric with significant effects from only one ENSO phase in most areas of the world [*Sun et al*., 2015].

Much attention has been paid to precipitation extremes in China based on observations [*Gemmer et al*., 2011; *You et al*., 2011; *Zhai et al*., 2005], global climate models (GCMs) [*Jiang et al*., 2015; *Li et al*., 2013], and regional climate models (RCMs) [*Gao et al*., 2002; *Qin and Xie*, 2016]. *Sillmann et al*. [2013a, 2013b] and *Jiang et al*. [2015] quantitatively evaluated the ability of GCMs based on the state-of-the-art Coupled Model Intercomparison Project Phase 5 (CMIP5) [*Taylor et al*., 2012] to simulate climate extremes and found that CMIP5 models generally could simulate extremes and their trends. *Wang et al*. [2012] provided an overview of climate extremes in China and noted that RCMs performed better at detecting precipitation extremes in China. *Qin and Xie* [2016] predicted the future precipitation extremes in China using the RegCM4 RCM from the Abdus Salam International Center for Theoretical Physics (ICTP) [*Giorgi et al*., 2012] and discussed the possible underlying mechanism. Many studies have focused on the impacts of the SST on the mean precipitation or precipitation extremes over river basins in China [*Zhang et al*., 2016], but few have considered the precipitation extremes in the whole of China, especially in the arid and semiarid regions of Northwest China.

In this study, we aimed to elucidate the connections between the precipitation extremes during 1953–2002 in the dry and wet regions of China (see section 2 for definitions) and the SST of the eastern tropical Pacific Ocean (ETP; including the ENSO 1.2, 3, and 3.4 regions; bold sea green box in Figure S3 in the supporting information) using two sets of observations, 17 CMIP5 models (see Table 1 for details), and nine RCMs, where the results were downscaled by RegCM4 with different GCM initial and boundary conditions and different experimental setups. The extreme precipitation indices (R95p, Rx5day, and SDII; see Table 2) came from the Expert Team on Climate Change Detection and Indices (ETCCDI) [*Karl and Easterling*, 1999], and they were calculated using a modified code by us based on the package from ETCCDI, which could easily deal with different CMIP5 results with different calendar type. We determined the linear regression coefficients for the precipitation extremes over the dry and wet regions of China versus the SST of the ETP. We then analyzed

Table 2. Precipitation Extreme Indices Used in This Study, as Defined by the ETCCDI

ID	Index Name	Index Definitions	Units
R95p	Very heavy precipitation	Total precipitation for days with precipitation above 95th percentile	mm
Rx5day	Maximum 5 day precipitation	Maximum consecutive 5 day precipitation	mm
SDII	Simple daily intensity	Mean precipitation on wet days with precipitation ≥1 mm	mm d^{-1}

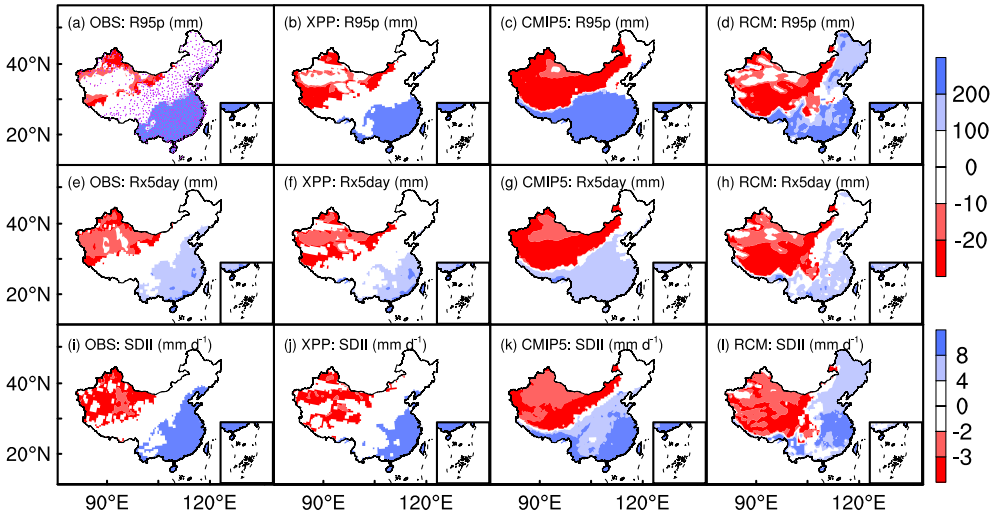

Figure 1. Spatial patterns of the average of precipitation extremes (R95p, Rx5day, and SDII) determined with 5 year low-pass Lanczos filtering in China for the (a, e, and i) OBS, (b, f, and j) XPP, (c, g, and k) ensemble of CMIP5 models, and (d, h, and l) ensemble of RCM models. The locations of the OBS stations are marked by purple dots. The extremes in the dry region are marked as negative values to clearly indicate both the dry and wet regions.

the correlations between the extreme indices and the SST of the ETP based on observations, CMIP5 models, and the RCM results.

2. Data, Models, and Methods

2.1. Data

In this study, we used two sets of daily precipitation observations: a set obtained from 753 meteorological stations during 1951–2004 (referred to as OBS; see Figure 1a for the locations of the stations) provided by the Chinese Meteorological Administration [*Xie et al.*, 2007b], and the other set comprised gauge-based daily precipitation values obtained at a resolution of 0.5° × 0.5° over East Asia from 1982 to 2002 (referred to as XPP) [*Xie et al.*, 2007a]. The historical daily precipitation results from 17 CMIP5 models (ACCESS1.0, BCC-CSM1.1, BNU-ESM, CanESM2, CCSM4, CESM1-BGC, CNRM-CM5, CSIRO-Mk3.6.0, FGOALS-g2, FGOALS-s2, GFDL-ESM2M, HadGEM2-ES, IPSL-CM5A-LR, MIROC-ESM-CHEM, MPI-ESM-LR, MRI-CGCM3, and NorESM1-M) from as many institute as possible were also employed to study precipitation extremes (Table 1). Because long time simulation by RegCM4 requires expensive calculations and large storage volume, we used RegCM4 only downscaling three CMIP5 models (GFDL_ESM2M, HadGEM2-ES, and IPSL-CM5A-LR) with different land surface processes and different convection precipitation schemes, thereby yielding nine sets of RCM results (the models and experiment setups are described in section 2.2).

The observed monthly SST was obtained from the Hadley Centre Sea Ice and Sea Surface temperature (HadSST) data set with a resolution of 1° [*Rayner et al.*, 2003]. The monthly mean SST outputs from the 17 CMIP5 models (Table 2) described previously were used to determine the relationships with the precipitation extremes based on the corresponding CMIP5 models. All the data sets of the monthly SST were averaged to annual time series. It should be noted that the precipitation extremes obtained from RCMs are produced with the SST output from the forcing CMIP5 model although the related SST is not influenced by the RCM-simulated regional climate as an initial boundary condition.

The data sets used in this study ranged from 1951 to 2004 for OBS and CMIP5 models and from 1982 to 2004 for RCMs, and the XPP ranged from 1982 to 2002. First, all the daily precipitation data sets were regridded to 140 × 80 longitude-latitude grids with a resolution of 0.5° by linear interpolation with the distance weight to facilitate comparisons. The SST data sets were regridded to 1° × 1° using the same interpolation method.

2.2. RCM Models and Experimental Setup

The RCM used to downscale the CMIP5 results was ICTP RegCM4 [*Giorgi et al.*, 2012], which has a dynamical core based on the fifth-generation mesoscale modeling system [*Grell et al.*, 1994]. The initial and boundary

conditions were generated from three CMIP5 models (GFDL_ESM2M, HadGEM2-ES, and IPSL-CM5A-LR). To reduce the calculation and storage costs, RegCM4 was integrated for 24 years from 1 January 1981 to 31 December 2004 over East Asia, where it was centered at (36°N, 102°E) with 120 × 90 longitude-latitude grids at a resolution of 60 km with 23 vertical layers. The land surface component of RCM was adopted as Community Land Model (CLM) [*Steiner et al*., 2009], and the convection scheme was the Grell scheme with Fritsch and Chappel closure [*Grell*, 1993], or the Massachusetts Institute of Technology (MIT) [*Emanuel and Zivkovic-Rothman*, 1999] or Biosphere-Atmosphere Transfer Scheme (BATS) [*Dickinson et al*., 1993] schemes together with the Grell scheme as the convection scheme.

2.3. Identifying the Dry and Wet Regions of China

We calculated the annual time series of precipitation extremes R95p (threshold indices), Rx5day (absolute indices), and SDII (average indices) for OBS, XPP, each CMIP5, and the RCM result using modified package from ETCCDI which could easily deal with different CMIP5 results. First, to better reflect the connections between the time series of extremes for the long period and the SST, both the extremes and the SST data sets were filtered using the 5 year low-pass Lanczos filtering method [*Duchon*, 1979] to remove data frequencies greater than once in 5 years, where the weights are defined by $w_k = \frac{\sin(2\pi fk)}{\pi k}\frac{\sin(\pi k/n)}{\pi k/n}$, where $2 \times n + 1$ is the number of the weights and f is the cutoff frequency. Thus, the filtered precipitation extreme indices and SST data sets for the CMIP5 models and OBS ranged from 1953 to 2002 and from 1984 to 2002 for the RCM models, and the extreme indices in XPP ranged from 1984 to 2000.

For each extreme index, the dry and wet grid cells were identified based on the multiyear mean precipitation extremes from 1984 to 2002 for OBS, XPP (from 1984 to 2000), each CMIP5, and the RCM data. The grid cells with the lowest 30% nonmissing precipitation extreme indices were regarded as the dry region, and those with the highest 30% comprised the wet region. Before investigating the connections between the precipitation extremes and the SST, the linear trends and climatology means were then removed for each extreme index as well as the SST over each grid cell in each set to reflect the connections between the extreme indices and the natural variability in the SST. We then did Shapiro-Wilk test of normality for each annual time series of extreme indices over each grid by the statistics software R (https://www.r-project.org/) and found that the R95p for OBS passed the normality test at p level of 0.1 over 49.7% of all grids with nonmissing values, 69.6% for XPP, ranged from 53.6% to 79.2% for CMIP5s, and ranged from 37.0% to 80.8% for RCMs (Figure S1 in the supporting information). And the other precipitation extremes showed similar results. The indices were then normalized by dividing them by the corresponding standard deviation to ensure that the average was not dominated by the grid cells with large values when calculating the time series of the indices over the dry and wet regions.

3. Results

3.1. Precipitation Extremes Over the Dry and Wet Regions of China

We identified the dry and wet regions of China as those with the lowest 30% and highest 30% for each precipitation extreme index after filtering with a 5 year low-pass Lanczos filtering based on OBS, XPP, each CMIP5, and the RCM model results. The ensemble mean of precipitation extremes of 17 CMIP5 models were calculated by averaging precipitation extremes based on CMIP5 models, and a similar operation was made for the ensemble of RCM models. Figure 1 shows the spatial patterns of the precipitation extremes for the dry and wet regions of China based on OBS, XPP, the ensemble mean of 17 CMIP5 models, and the ensemble mean of nine RCM results. The lowest 30% of the precipitation extremes for each data set were marked as negative values to clearly show both the dry and wet regions in a single figure. For CMIP5 ensemble and RCMs ensemble more than 30% of the study area were marked as the dry or wet region which came from CMIP5 and RCMs ensemble spread, respectively (Figure 1). The dry regions with precipitation extreme indices obtained from both OBS (Figures 1a, 1e, and 1i) and XPP (Figures 1b, 1f, and 1j) were detected mainly in northwestern China, which contains arid and semiarid areas, whereas the wet regions were found in southeastern China, which is a humid area. The extreme indices based on the CMIP5 ensemble and RCM ensemble also exhibited similar patterns to the observations OBS and XPP, i.e., dry in northwestern China and wet in southeastern China, although the R95p and SDII values obtained from the RCM ensemble had a positive bias in northeastern China.

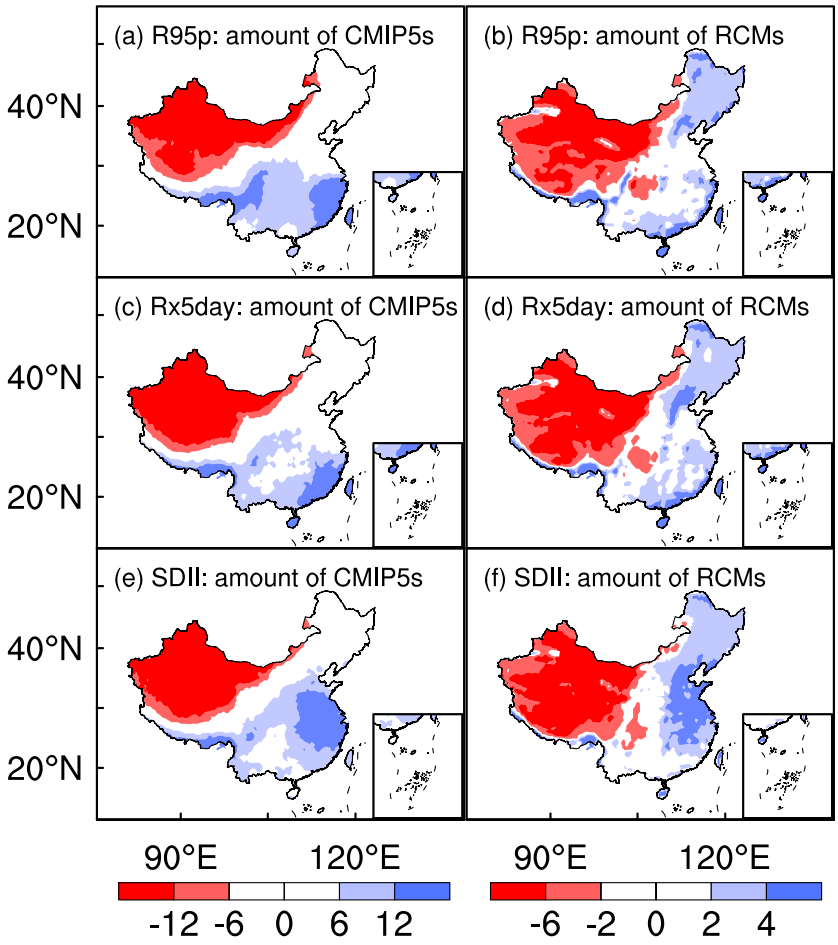

Figure 2. Spatial distributions of the areas identified as dry or wet grid regions by the (a, c, and e) CMIP5 models and (b, d, and f) RCM models for precipitation extremes (R95p, Rx5day, and SDII). The grid cells in the dry region are assigned negative values to clearly differentiate the dry and wet regions.

Figure 2 shows the spatial distributions of the areas identified by 17 CMIP5 models and nine RCM as dry (red color) and wet (blue color) grid cells. Dry grid cells were located in northwestern China identified by more than 12 CMIP5 models, while the identification of wet grid cells exhibited high spatial variability, where more than six CMIP5 models located the wet regions in southeastern China. Over 12 CMIP5 models identified wet grid cells for R95p and Rx5day in southeastern China along the coast, as well as for SDII in eastern China (Figures 2a, 2c, and 2e). More than six of nine RCM results also located the dry grid cells in northwestern China, but the RCMs exhibited high spatial variation when identifying the wet grid cells, where two to four RCM results identified the wet regions in northeastern China.

The CMIP5 and RCM models could simulate the temporal average and spatial patterns of the extreme indices throughout China as well as in the dry and wet regions to some extent, but there were large differences in the extreme precipitation indices obtained by the CMIP5 and RCM models and even among different observations (Figures 1 and 3 and Figure S2 in the supporting information). Compared with extreme indices based on the CMIP5 models, the temporal averages of extreme indices by RCM matched better with the observed indices, such as R95p (about 20 mm for OBS, 35 mm for XPP, 50 mm for the CMIP5 ensemble, and 40 mm for the RCM ensemble) and Rx5day (about 20 mm for OBS, 30 mm for XPP and the RCM ensemble, and 33 mm for the CMIP5 ensemble) in the dry region (Figures 3b and 3e), as well as the SDII throughout China and in the wet region (about 11 mm for both OBS and the RCM ensemble, 13 mm for XPP, and 9 mm for the CMIP5 ensemble) (Figures 3g and 3i), which probably reflected the RCM's higher temporal and spatial resolution of land surface processes and cumulus convection. Figure 4 shows the probability density distribution of the time series of precipitation extremes obtained from OBS, XPP, CMIP5 ensemble, and RCM ensemble in

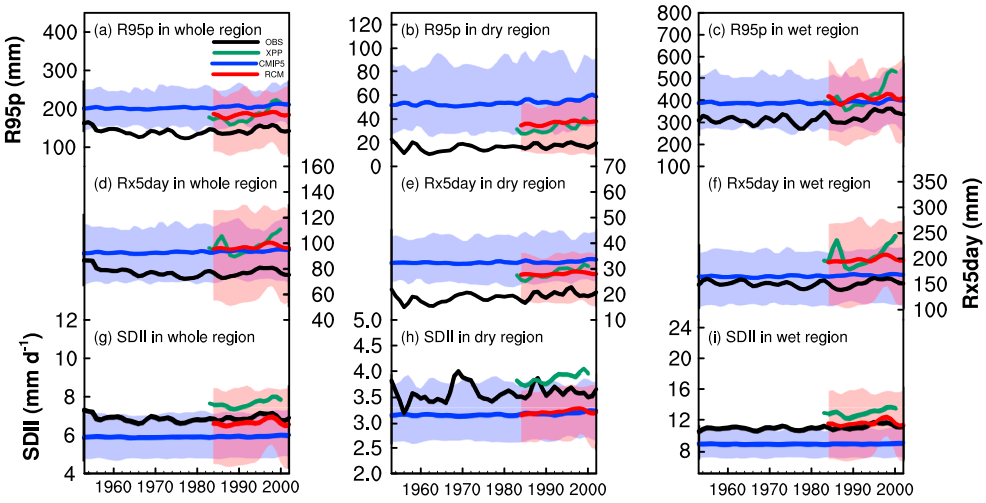

Figure 3. Time series of precipitation extremes (R95p, Rx5day, and SDII) with 5 year low-pass Lanczos filtering for the observations (OBS and XPP), ensemble of 17 CMIP5 models, and ensemble of nine RCM models for the (a, d, and g) whole of China, (b, e, and h) dry regions, and (c, f, and i) wet regions. The shaded colors for the CMIP5 ensemble and RCM ensemble represent the spreads of the 17 CMIP5 models and nine RCM models, respectively.

the dry and wet regions of China. The simulated extremes obtained from both the CMIP5 and RCM models had lower temporal variation than those based on observations (OBS and XPP) in the dry and wet regions, thereby indicating that care is needed when studying precipitation extremes with climate models. Compared with the CMIP5 models, the RCM models simulated extremes with lower temporal amplitude in the dry region, whereas in the wet region the variations in R95p and SDII were higher according to the RCM models.

3.2. Connections Between the Precipitation Extremes in the Dry and Wet Regions of China and the SST of the ETP

We calculated the correlations between the extreme indices and the SST, such as extremes for OBS and XPP and the observed SST HadSST, extremes for each CMIP5 model and the related annual series of the SST, and extremes for each RCM and the SST from the GCM which forced the RCM. The correlations exhibited high spatial variations, and the different indices in the dry and wet regions had different correlations with the

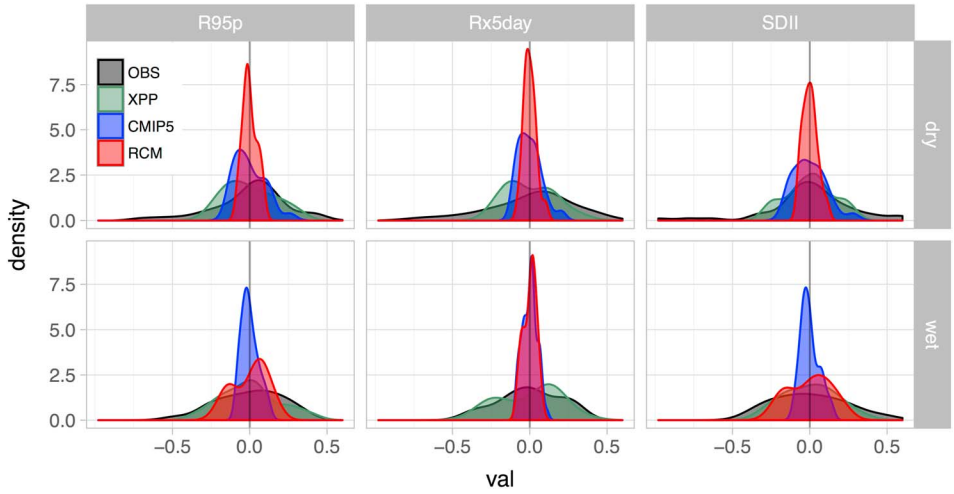

Figure 4. Probability density functions for the time series of normalized precipitation extremes (R95p, RX5day, and SDII) obtained by the OBS (1953–2002), XPP (1984–2000), ensemble of CMIP5 models (1953–2002), and ensemble of RCM models (1984–2002) in the dry and wet regions of China.

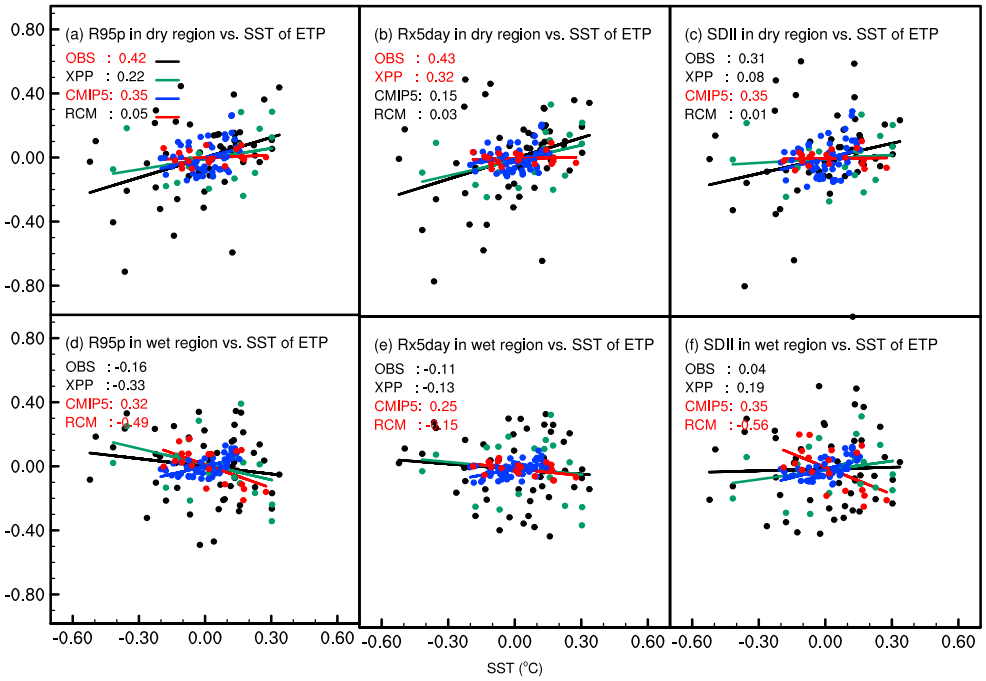

Figure 5. Scatterplots for the normalized annual time series of precipitation extreme indices (R95p, Rx5day, and SDII) in the (a–c) dry regions and (d–f) wet regions versus the SST in the ETP obtained from the observations (OBS and XPP), ensemble of 17 CMIP5 models, and ensemble of nine RCM models. The solid lines in Figures 5a–5f show the linear regression, where the slopes of the linear regression are denoted in red if they were significant at the $p < 0.1$ level according to a *t* test.

SST (Figure S3 in the supporting information). In this study, we focused mainly on the connections between the extreme indices and the SST of the ETP (20°S, 20°N) × (180°, 100°W), including the ENSO 1.2, 3, and 3.4 regions (bold green box in Figure S3), where there was high temporal variation in the SST (Figure S4), and it greatly affected the global climate [*McPhaden et al.*, 2006]. During 1953–2002, the detrended SST of the ETP was detected spread with a range of (−0.5°C, 0.3°C) for the observed SST and (−0.2°C, 0.2°C) for the CMIP5 models ensemble and the three CMIP5 models that forced the RCMs (Figure 5). Compared with the observed SST, the CMIP5-simulated SST had a lower amplitude.

In the dry region, all the extreme indices obtained from the two sets of observations, the ensemble of 17 CMIP5 models, and the ensemble of nine RCM models had positive regression coefficients versus the SST of the ETP (Figures 5a–5c). The regression coefficients for the extreme indices based on OBS versus the SST of the ETP were 0.42 for R95p, 0.43 for Rx5day, and 0.31 for SDII, which were significant at the $p < 0.1$ level for R95p and Rx5day. The RCM-simulated extreme indices in the dry region were predicted to increase with the SST but with smaller slopes (0.05 for R95p, 0.03 for Rx5day, and 0.01 for SDII) compared with those from OBS, XPP, and CMIP5 models ensemble, although the RCMs performed better at simulating the climatic precipitation extremes (Figures 3b and 3e and Figure S4 in the supporting information) than the CMIP5 models. Figure 6 shows the variations in the correlations between the ETP's SST and the extremes from CMIP5 models and RCM models. All the extremes in the dry regions had positive median correlation coefficients for CMIP5 and RCMs with the ETP's SST.

In contrast, to the good agreement among the positive regression coefficients of the extreme indices for the dry region versus the SST of the ETP, the connections between the extreme indices in the wet region and the SST were more complex (Figures 5d–5f). In the wet region, R95p had a negative linear relationship with the SST of the ETP with regression coefficients of −0.16 for OBS, −0.33 for XPP, and −0.49 for the RCM ensemble, whereas a positive linear relationship was found for the CMIP5 ensemble with a slope of 0.32. In addition, positive linear relationships between the SDII and SST were detected for OBS, XPP, and the CMIP5 ensemble, whereas the RCM ensemble had a moderate negative linear relationship, with a regression coefficient of −0.56. The observed values of Rx5day based on OBS and XPP had negative linear relationship

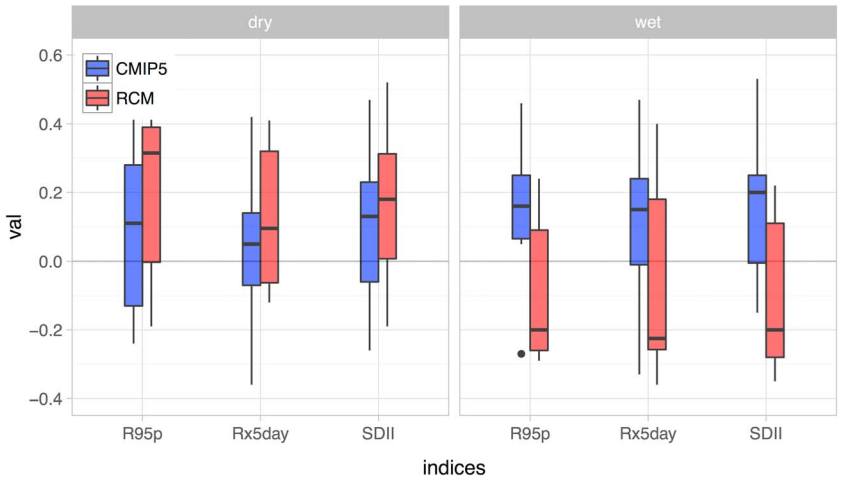

Figure 6. Box plots of the correlation coefficients between annual time series of precipitation extremes (R95p, RX5day, and SDII) obtained by the ensembles of 17 CMIP5 models (blue) and nine RCM models (red) in the (left) dry region and (right) wet region of China versus the SST in the ETP. The lower and upper "hinges" represent the 25th and 75th percentiles, and the line in the box means the median of the data sets. The upper/lower whisker extends the hinge to the maximum/minimum value of the data sets that is within 1.5 times interquartile range, or interquartile range. Data outside the upper and lower whiskers are plotted as points.

with the SST as well as those obtained using the RCM ensembles (Figure 5e). In general, in the wet region, the CMIP5 simulated extremes were positively correlated with the ETP's SST, whereas the opposite was found for the RCM models (Figure 6).

Due to the large spreads obtained by the 17 CMIP5 models and nine RCM models, we also analyzed the correlations between the precipitation extreme indices in the dry and wet regions based on the observations, CMIP5 models, and RCM results versus the corresponding SST of the ETP (Figure 7). There was good agreement in the positive correlations for the precipitation extremes in the dry region by OBS, XPP, CMIP5 ensemble, and RCM ensemble versus the SST of the ETP, but the different CMIP5 models had large variations, e.g., FGOALS-g2, MRI-CGCM3, and NorESM1-M yielded moderate negative correlations between the extreme indices and the SST, whereas BNU-ESM, GFDL-ESM2M, and MPI-ESM-LR had large significant positive correlations at the $p < 0.1$ level. Most of the RCM models yielded positive correlations between the extreme indices in the dry region and the SST, such as RCM_HadGEM2_CLM and RCM_HadGEM2_Grell when run using the RCM with land surface component CLM3.5 forced by HadGEM2, as well as using the MIT and Grell convection

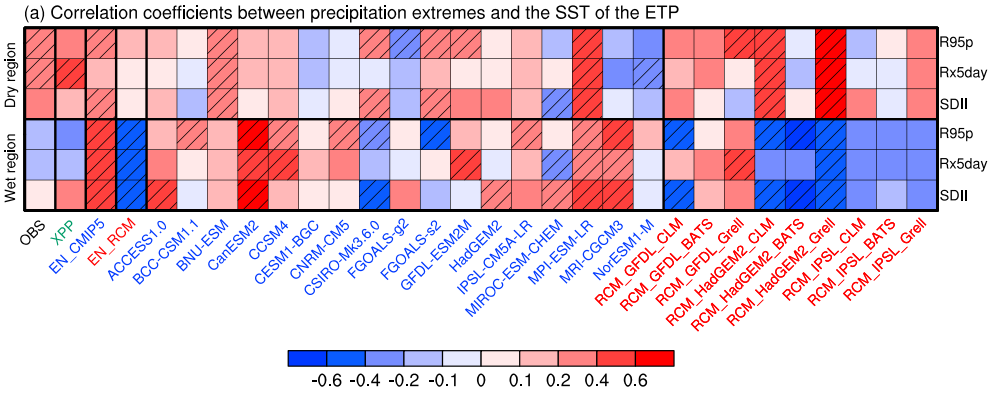

Figure 7. Correlations among the annual time series of precipitation extreme indices in the dry and wet regions of China based on the observations (OBS and XPP), 17 CMIP5 models and their ensemble, and nine RCM models and their ensemble versus the corresponding SST in the ETP. EN_CMIP5 is the correlation with the ensemble of 17 CMIP5 models, and EN_RCM is the correlation with the ensemble of nine RCM models. The shaded boxes show the significant correlations at the $p < 0.1$ level.

precipitation schemes. Seven of the nine RCM models had negative correlations with the SST, and thus, there was a significant negative correlation with the RCM ensemble. Due to the lack of feedback from the regional climate to the SST when running the RCMs, RCMs might present worse relationship between the precipitation extremes and the SST compare with CMIP5 models.

4. Conclusions

In this study, we first identified the dry and wet regions of China based on each of the extreme precipitation indices using 5 year low-pass Lanczos filtering for two sets of observations, 17 CMIP5 models, and nine RCM models. The dry region comprised the grid cells with the lowest 30% of the nonmissing extreme indices, which were located in northwestern China, and the wet region comprised grid cells with the highest 30% of the extreme indices, which were generally located in southeastern China. Compared with the observations (OBS and XPP), the CMIP5 ensemble and RCM ensemble could simulate the temporal changes in extreme indices in the dry and wet regions to some extent, but there were some biases in the extreme ndices obtained from the CMIP5 and RCM models. Compared with the temporal average of the extreme indices simulated by the CMIP5 model, those simulated by the RCMs matched better with the observed indices determined by OBS and XPP, such as the values of R95p and Rx5day in the dry region and SDII in the wet region.

After test of normality for each annual time series of extreme indices over each spatial grid, the indices were then normalized by dividing them by the corresponding standard deviation to ensure that the average was not dominated by the grid cells with large values. We then studied the relationships between the precipitation extreme indices in the dry and wet regions versus the SST of the ETP. In the dry region of China, the precipitation extreme indices based on the observations, CMIP5 ensemble, and RCM ensemble had positive linear relationships with the SST of the ETP, whereas for the wet region of China, the linear relationships between the extreme indices and the SST were more complex, with a negative regression coefficient for R95p and a positive regression coefficient for SDII based on the two sets of observations versus the SST of the ETP.

After comparing the correlations between the precipitation extremes and the corresponding SST, we found large variations with different CMIP5 models, thereby suggesting that it might be better to detect the connections between the extreme indices and the SST by using an ensemble of "good" CMIP5 models that obtain better performance at simulating precipitation extremes. The same problem occurred for the RCM models, which might have been caused by the lack of interaction between the regional climate and the SST when running the RCMs, although the RCMs generally performed better at simulating the temporal average and spatial patterns of precipitation extremes.

The possible mechanisms responsible for the effects of the SST in the ETP on precipitation extremes in China would be discussed in the following work through the variables such as specific humidity and horizontal/vertical wind in the period when precipitation extremes occur.

Acknowledgments

We thank the Editor, L. Ruby Leung, and the reviewers for their careful and professional suggestions that help to improve the quality of this manuscript so much. This study was supported by the National Natural Science Foundation of China (grant 41575096) and by the Chinese Academy of Sciences Strategic Priority Research Program (grant XDA05110102). The station-based daily precipitation data was provided by the Chinese Meteorological Administration (http://www.cma.gov.cn). The gauge-based daily precipitation data were provided by *Xie et al.* [2007a]. The observed monthly SST was obtained from the Hadley Centre Sea Ice and Sea Surface temperature data set (HadSST, http://www.metoffice.gov.uk/hadobs/hadsst3/data/download.html). The daily precipitation and the sea surface temperature data by the CMIP5 models were downloaded from https://esgf-node.llnl.gov/search/cmip5 under the World Climate Research Programme (WCRP). The ETCCDI indices were calculated based on fclimdex package (http://etccdi.pacificclimate.org). RCM results could be accessed from http://www.escience.cn/people/pqin/admin/p/JGR-2017.

References

Alexander, L. V., P. Uotila, and N. Nicholls (2009), Influence of sea surface temperature variability on global temperature and precipitation extremes, *J. Geophys. Res.*, *114*, D18116, doi:10.1029/2009JD012301.

Allan, R. P., and B. J. Soden (2008), Atmospheric warming and the amplification of precipitation extremes, *Science*, *321*(5895), 1481–1484, doi:10.1126/science.1160787.

Bellprat, O., and F. Doblas-Reyes (2016), Attribution of extreme weather and climate events overestimated by unreliable climate simulations, *Geophys. Res. Lett.*, *43*, 2158–2164, doi:10.1002/2015GL067189.

Castello, A. F., and M. L. Shelton (2004), Winter precipitation on the US Pacific Coast and El Niño Southern Oscillation events, *Int. J. Climatol.*, *24*(4), 481–497, doi:10.1002/joc.1011.

Chan, S. C., E. J. Kendon, N. M. Roberts, H. J. Fowler, and S. Blenkinsop (2016), Downturn in scaling of UK extreme rainfall with temperature for future hottest days, *Nat. Geosci.*, *9*, 24–28, doi:10.1038/ngeo2596.

Dai, A., and T. M. L. Wigley (2000), Global patterns of ENSO-induced precipitation, *Geophys. Res. Lett.*, *27*(9), 1283–1286, doi:10.1029/1999GL011140.

Dickinson, R. E., A. Henderson-Sellers, and P. Kennedy (1993), Biosphere-Atmosphere Transfer Scheme (BATS) version 1e as coupled to the NCAR community climate model, *Tech Note NCAR.TN-387+STR*.

Donat, M. G., et al. (2013), Updated analyses of temperature and precipitation extreme indices since the beginning of the twentieth century: The HadEX2 dataset, *J. Geophys. Res. Atmos.*, *118*, 2098–2118, doi:10.1002/jgrd.50150.

Donat, M. G., et al. (2014), Changes in extreme temperature and precipitation in the Arab region: Long-term trends and variability related to ENSO and NAO, *Int. J. Climatol.*, *34*, 581–592, doi:10.1002/joc.3707.

Donat, M. G., A. L. Lowry, L. V. Alexander, P. A. O'Gorman, and N. Maher (2016), More extreme precipitation in the world's dry and wet regions, *Nat. Clim. Change*, *6*(5), 508–513, doi:10.1038/nclimate2941.

Duchon, C. E. (1979), Lanczos filtering in one and two dimensions, *J. Appl. Meteorol.*, *18*(8), 1016–1022, doi:10.1175/1520-0450(1979)018<1016:LFIOAT>2.0.CO;2.

Emanuel, K. A., and M. Zivkovic-Rothman (1999), Development and evaluation of a convection scheme for use in climate models, *J. Atmos. Sci.*, *56*(11), 1766–1782, doi:10.1175/1520-0469(1999)056<1766:DAEOAC>2.0.CO;2.

Gao, X. J., Z. C. Zhao, and F. Giorgi (2002), Changes of extreme events in regional climate simulations over East Asia, *Adv. Atmos. Sci.*, *19*(5), 927–942.

Gemmer, M., T. Fischer, T. Jiang, B. D. Su, and L. L. Liu (2011), Trends in precipitation extremes in the Zhujiang River Basin, South China, *J. Clim.*, *24*(3), 750–761, doi:10.1175/2010JCLI3717.1.

Giorgi, F., et al. (2012), RegCM4: Model description and preliminary tests over multiple CORDEX domains, *Clim. Res.*, *52*(1), 7–29, doi:10.3354/cr01018.

Grell, G. A. (1993), Prognostic evaluation of assumptions used by cumulus parameterizations, *Mon. Weather Rev.*, *121*(3), 764–787, doi:10.1175/1520-0493(1993)121<0764:PEOAUB>2.0.CO;2.

Grell, G. A., J. Dudhia, and D. R. Stauffer (1994), A description of the fifth generation Penn State/NCAR Mesoscale Model (MM5), *NCAR Tech. Note TN-398 STR*, 121 pp.

Grimm, A. M. (2011), Interannual climate variability in South America: Impacts on seasonal precipitation, extreme events, and possible effects of climate change, *Stochastic Environ. Res. Risk Assess.*, *25*(4), 537–554, doi:10.1007/s00477-010-0420-1.

Huang, P., and S. P. Xie (2015), Mechanisms of change in ENSO-induced tropical Pacific rainfall variability in a warming climate, *Nat. Geosci.*, *8*(12), 922–926, doi:10.1038/ngeo2571.

IPCC (2012), *Managing the Risks of Extreme Events and Disasters to Advance Climate Change Adaptation. A Special Report of Working Groups I and II of the Intergovernmental Panel on Climate Change*, 582 pp., Cambridge Univ. Press, Cambridge, U. K., and New York.

Jiang, Z. H., W. Li, J. J. Xu, and L. Li (2015), Extreme precipitation indices over China in CMIP5 models. Part I: Model evaluation, *J. Clim.*, *28*(21), 8603–8619, doi:10.1175/JCLI-D-15-0099.1.

Karl, T. R., and D. R. Easterling (1999), Climate extremes: Selected review and future research directions, *Clim. Change*, *42*(1), 309–325, doi:10.1007/978-94-015-9265-9_17.

Li, J. F., Q. Zhang, Y. D. Chen, and V. P. Singh (2013), GCMs-based spatiotemporal evolution of climate extremes during the 21st century in China, *J. Geophys. Res. Atmos.*, *118*, 11,017–11,035, doi:10.1002/jgrd.50851.

Martin, E. R., C. Thorncroft, and B. B. B. Booth (2014), The multidecadal Atlantic SST-Sahel rainfall teleconnection in CMIP5 simulations, *J. Clim.*, *27*(2), 784–806, doi:10.1175/JCLI-D-13-00242.1.

McPhaden, M. J., S. E. Zebiak, and M. H. Glantz (2006), ENSO as an integrating concept in Earth science, *Science*, *314*(5806), 1740–1745, doi:10.1126/science.1132588.

Meehl, G. A., C. Tebaldi, H. Teng, and T. C. Peterson (2007), Current and future US weather extremes and El Niño, *Geophys. Res. Lett.*, *34*, L20704, doi:10.1029/2007GL031027.

O'Gorman, P. A. (2012), Sensitivity of tropical precipitation extremes to climate change, *Nat. Geosci.*, *5*(10), 697–700.

O'Gorman, P. A., and T. Schneider (2009), The physical basis for increases in precipitation extremes in simulations of 21st-century climate change, *Proc. Natl. Acad. Sci.*, *106*(35), 14,773–14,777, doi:10.1073/pnas.0907610106.

Qin, P. H., and Z. H. Xie (2016), Detecting changes in future precipitation extremes over eight river basins in China using RegCM4 downscaling, *J. Geophys. Res. Atmos.*, *121*, 6802–6821, doi:10.1002/2016JD024776.

Rayner, N. A., D. E. Parker, E. B. Horton, C. K. Folland, L. V. Alexander, D. P. Rowell, E. C. Kent, and A. Kaplan (2003), Global analyses of sea surface temperature, sea ice, and night marine air temperature since the late nineteenth century, *J. Geophys. Res.*, *108*(D14), 4407, doi:10.1029/2002JD002670.

Seager, R., N. Harnik, W. A. Robinson, Y. Kushnir, M. Ting, H. P. Huang, and J. Velez (2005), Mechanisms of ENSO-forcing of hemispherically symmetric precipitation variability, *Q. J. R. Meteorol. Soc.*, *131*(608), 1501–1527, doi:10.1256/qj.04.96.

Shi, X. M., and D. Durran (2016), Sensitivities of extreme precipitation to global warming are lower over mountains than over oceans and plains, *J. Clim.*, doi:10.1175/JCLI-D-15-0576.1.

Sillmann, J., V. V. Kharin, X. Zhang, F. W. Zwiers, and D. Bronaugh (2013a), Climate extremes indices in the CMIP5 multimodel ensemble: Part 1. Model evaluation in the present climate, *J. Geophys. Res. Atmos.*, *118*, 1716–1733, doi:10.1002/jgrd.50203.

Sillmann, J., V. V. Kharin, F. W. Zwiers, X. Zhang, and D. Bronaugh (2013b), Climate extremes indices in the CMIP5 multimodel ensemble: Part 2. Future climate projections, *J. Geophys. Res. Atmos.*, *118*, 2473–2493, doi:10.1002/jgrd.50188.

Steiner, A. L., J. S. Pal, S. A. Rauscher, J. L. Bell, N. S. Diffenbaugh, A. Boone, L. C. Sloan, and F. Giorgi (2009), Land surface coupling in regional climate simulations of the West African monsoon, *Clim. Dyn.*, *33*(6), 869–892, doi:10.1007/s00382-009-0543-6.

Sun, C., J. P. Li, and R. Q. Ding (2016), Strengthening relationship between ENSO and western Russian summer surface temperature, *Geophys. Res. Lett.*, *43*, 843–851, doi:10.1002/2015GL067503.

Sun, X., B. Renard, M. Thyer, S. Westra, and M. Lang (2015), A global analysis of the asymmetric effect of ENSO on extreme precipitation, *J. Hydrol.*, *530*, 51–65, doi:10.1016/j.jhydrol.2015.09.016.

Taylor, K. E., R. J. Stouffer, and G. A. Meehl (2012), An overview of CMIP5 and the experiment design, *Bull. Am. Meteorol. Soc.*, *93*(4), 485–498, doi:10.1175/BAMS-D-11-00094.1.

Tian, Q., M. Prange, and U. Merkel (2016), Precipitation and temperature changes in the major Chinese river basins during 1957–2013 and links to sea surface temperature, *J. Hydrol.*, *536*, 208–221, doi:10.1016/j.jhydrol.2016.02.048.

Ummenhofer, C. C., A. Sen Gupta, M. H. England, A. S. Taschetto, P. R. Briggs, and M. R. Raupach (2015), How did ocean warming affect Australian rainfall extremes during the 2010/2011 La Niña event?, *Geophys. Res. Lett.*, *42*, 9942–9951, doi:10.1002/2015GL065948.

Volosciuk, C., D. Maraun, V. A. Semenov, N. Tilinina, S. K. Gulev, and M. Latif (2016), Rising Mediterranean Sea surface temperatures amplify extreme summer precipitation in Central Europe, *Sci Rep-Uk*, *6*, doi:10.1038/srep32450.

Wang, H. J., J. Q. Sun, H. P. Chen, Y. L. Zhu, Y. Zhang, D. B. Jiang, X. M. Lang, K. Fan, E. T. Yu, and S. Yang (2012), Extreme climate in China: Facts, simulation and projection, *Meteorol. Z.*, *21*(3), 279–304, doi:10.1127/0941-2948/2012/0330.

Xie, P. P., A. Yatagai, M. Y. Chen, T. Hayasaka, Y. Fukushima, C. M. Liu, and S. Yang (2007a), A gauge-based analysis of daily precipitation over East Asia, *J. Hydrometeorol.*, *8*(3), 607–626, doi:10.1175/JHM583.1.

Xie, Z. H., F. Yuan, Q. Y. Duan, J. Zheng, M. L. Liang, and F. Chen (2007b), Regional parameter estimation of the VIC land surface model: Methodology and application to river basins in China, *J. Hydrometeorol.*, *8*(3), 447–468, doi:10.1175/Jhm568.1.

Yoon, J. H., S. Y. S. Wang, R. R. Gillies, B. Kravitz, L. Hipps, and P. J. Rasch (2015), Increasing water cycle extremes in California and in relation to ENSO cycle under global warming, *Nat. Commun.*, *6*, 8657, doi:10.1038/ncomms9657.

You, Q. L., S. C. Kang, E. Aguilar, N. Pepin, W. A. Flugel, Y. P. Yan, Y. W. Xu, Y. J. Zhang, and J. Huang (2011), Changes in daily climate extremes in China and their connection to the large scale atmospheric circulation during 1961–2003, *Clim. Dyn.*, *36*(11), 2399–2417, doi:10.1007/s00382-009-0735-0.

Zhai, P. M., X. B. Zhang, H. Wan, and X. H. Pan (2005), Trends in total precipitation and frequency of daily precipitation extremes over China, *J. Clim.*, *18*(7), 1096–1108, doi:10.1175/JCLI-3318.1.

Zhang, Q., Y. Wang, V. P. Singh, X. H. Gu, D. D. Kong, and M. Z. Xiao (2016), Impacts of ENSO and ENSO Modoki plus A regimes on seasonal precipitation variations and possible underlying causes in the Huai River basin, China, *J. Hydrol.*, *533*, 308–319, doi:10.1016/j.jhydrol.2015.12.003.